Proceedings of ASME Turbo Expo 2025
Turbomachinery Technical Conference and Exposition
GT2025
June 16–20, 2025, Memphis, Tennessee

GT2025-152405

AN EXPERIMENTAL INVESTIGATION INTO PARTICLE DEPOSITION IN DOUBLE-WALL EFFUSION COOLING SYSTEMS

Michael van de Noort*
Dept. of Engineering Science
University of Oxford
Oxford, OX1 3PJ, United Kingdom
michael.vandenoort@eng.ox.ac.uk

Charlie Hickling
Turbines
Rolls-Royce PLC.
Bristol, BS34 7QE, United Kingdom
charlie.hickling@rolls-royce.com

Florian Y. A. Villain
Dept. of Engineering Science
University of Oxford
Oxford, OX1 3PJ, United Kingdom
florian.villain@eng.ox.ac.uk

Peter T. Ireland
Dept. of Engineering Science
University of Oxford
Oxford, OX1 3PJ, United Kingdom
peter.ireland@eng.ox.ac.uk

David R. H. Gillespie
Dept. of Engineering Science
University of Oxford
Oxford, OX1 3PJ, United Kingdom
david.gillespie@eng.ox.ac.uk

Janendra C. Telisinghe
Turbines
Rolls-Royce PLC.
Bristol, BS34 7QE, United Kingdom
janendra.telisinghe@rolls-royce.com

ABSTRACT

As Turbine Entry Temperatures of modern aeroengines continue to rise in pursuit of greater turbine thermal efficiencies, increasingly innovative and complex cooling systems are required to maintain turbine component temperatures at acceptable levels. Double-Wall Effusion Cooling Systems are one possible answer to this challenge – by combining dense arrays of impingement holes and pedestals for internal cooling with tightly packed effusion holes for external cooling, high metal cooling effectiveness can be achieved at relatively low rates of coolant consumption. However, the intricate nature of these cooling schemes leaves them vulnerable to the deposition of ingested particulate matter, which can eventually lead to cooling passage blockage and the failure of the cooling system.

This paper details an experimental investigation into four factors affecting deposition: the metal temperature, the cooling system geometry, the particulate matter's composition, and the metal the cooling system is produced from. These tests were carried out using the Oxford Thermofluids Institute's High Temperature Rig, capable of operating at metal temperatures exceeding 1200 K. Deposition was evaluated both in terms of the proportion of inputted particulate matter that adhered to the metal surface, and where said deposition took place – the latter of which was done using a 3D Profilometer. Results are used to identify situations where measures would need to be put in place to limit the ingestion of particles into the turbine's secondary air system. In particular, deposition rates are seen to increase as the metal temperature increases, and as the impingement spacing to diameter ratio decreases.

* All correspondence to this author.

Keywords: Double-Wall Effusion Cooling, Particle Deposition, Blockage

NOMENCLATURE

D	Diameter (m)
L	Length (m)
r	Distance from Impingement Point (m)
Re	Reynolds Number
s	Spacing (m)
T	Temperature (K)
U	Uncertainty
x	Microscope Sampling Increment (Streamwise Direction) (m)
y	Microscope Sampling Increment (Spanwise Direction) (m)
z	Microscope Scanned Height (m)
η_m	Metal Cooling Effectiveness

Subscripts

c	Coolant
f	Effusion
i	Impingement
m	Metal
p	Pedestal
θ	Circumferential Average
∞	Mainstream

1. INTRODUCTION

As the need for increased thermal efficiencies in the aeroengine sector increases, demand is heating up for cooling systems that can sustain turbine components at levels that ensure a sufficient component life. Modern turbine cooling systems must prevent the degradation of components that are exposed to mainstream gas temperatures exceeding 2000 K [1], and must do so whilst limiting the consumption of coolant air to as low a level as possible – air that enters the secondary air system cannot be used in the combustor, limiting the engine's power, and when coolant is discharged back into the turbine's mainstream flow it incurs heavy aerodynamic penalties. These requirements have seen a general move toward transpiration and "transpiration-like" cooling systems [2], which Bunker estimated could reduce coolant consumption by 15-20% from the current state of the art.

One transpiration-like cooling system is Double-Wall Effusion Cooling in which a component is internally cooled by impingement and pin-fin cooling, and externally cooled by effusion cooling. The combination of the three systems can produce a high level of metal cooling effectiveness (1). One such example of a Double-Wall Effusion Cooling System is shown in Figure 1.

$$\eta_m = \frac{T_m - T_c}{T_\infty - T_c} \tag{1}$$

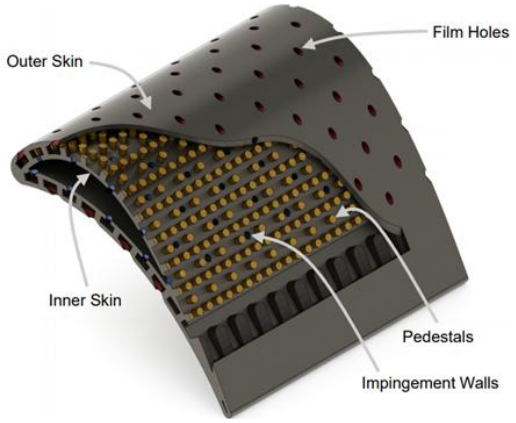

FIGURE 1: TURBINE BLADE USING DOUBLE-WALL EFFUSION COOLING SCHEME [3]

As the cooling system's geometry moves closer to transpiration, it has become increasingly intricate, with ever smaller hole diameters and more tightly packed arrays of holes and pedestals. This makes the cooling passages of Double-Wall Effusion Cooling Systems vulnerable to blockage by the deposition of particles that have been ingested into the secondary air systems. Ingested particle matters can include volcanic ash, atmospheric dust and sand. Significant amounts of deposition can lower cooling effectiveness and, when cooling holes are blocked, the creation of hot spots and the rapid failure of the component. As such, it is key for aeroengine cooling system designers to know the likelihood and susceptibility of their cooling systems to particle deposition.

In this paper, the influence of four key variables on particle deposition in Double-Wall Effusion cooling systems is investigated experimentally. These variables are the metal temperature, the cooling system geometry, the particle matter composition, and the specific metal alloy. The mass deposition is evaluated by the change in test piece mass, whilst the volume deposition is evaluated using a 3D Profilometer. It is shown that a high metal temperature, a low impingement hole spacing to diameter ratio, and a high particle concentration can combine to produce a high rate of deposition, such that the cooling system can be vulnerable to complete blockage between the two walls within an expected component life.

2. RELATED WORK

As Double-Wall cooling concepts have existed going back to the 1970s, there is a well-developed literature on the concept of Double-Wall Effusion Cooling as a system and significantly greater amount on each of its three constituent cooling systems. Many studies from the Oxford Thermofluids Institute's Cooling Research group (e.g. [3, 4, 5]) have highlighted the exceptional performance these systems can be capable of. Advanced concepts include triple wall designs [6], novel pedestals including stars and dimpled spheres [7], and complex lattice structures [8]. It is the intricate and complex nature of these designs, however, that lead to the vulnerability of these cooling systems to blockage by particle deposition.

The causes and effects of particulate deposition in gas turbines are increasingly well covered in the literature. Suman et al. [9] presented a comprehensive review of previous studies on particle behaviour under a wide range of gas turbine-representative conditions. This section will concentrate on the specific variables investigated in this study.

The composition of particles – both in size and chemical make-up – is well known to impact deposition rates. Studies of particle-laden free jet onto blades and vanes by Crosby et al. [10] and Bonilla et al. [11] respectively found that deposition in gas turbine components increased as the particle diameter increased. In the context of an effusion cooling geometry, however, Wolff et al. [12] found that smaller particulates (below 3 µm in diameter) had a greater propensity to stick on the hole surface, whilst larger particles had more of a ballistic impact and were less likely to deposit.

The chemical and physical composition of a particulate matter can heavily influence deposition, partly due to how the chemical composition affects its softening temperature. In the context of particulate matter being ingested by a full engine, certain chemical and physical properties will make particles more likely to be broken up or to deposit at earlier stages of the compressor, whilst others are more likely to be carried through to the hot section of the turbine. This variation was explored by Elms et al. [13], who conducted engine ingestion tests followed by chemical analysis to examine it. Composition effects can also include particle shape – the wide variation possible, and its effects, are well demonstrated in the work of Crowe & Bons [14].

Bons et al. [15] experimentally investigated the deposition of Arizona Road Dust for a cold-side impinging jet test. Results

showed that the capture efficiency (the proportion of loaded particulate matter which deposited onto the target surface) increased with both the temperature of the airflow that carried it and the wall temperature. It was noted that the rate of increase of the capture efficiency with temperature was approximately double for a rising fluid temperature than for a rising solid temperature.

Land et al. [16] studied how the impingement spacing to hole diameter ratio for a double wall system without pedestals impacted the amount of particulate deposition and the subsequent blockage of coolant flow. An optimal spacing to hole diameter ratio of 3.13 was found – at lower spacings, crossflow between the walls affected impingement jets which would otherwise "promote particle breakup", whereas at higher spacings impingement jets would spread out, losing velocity and thus be less effective at breaking up areas of deposition. In a more recent paper, McFerran et al. [17] experimentally examined the reduction in flow rate and heat transfer in Double-Wall combustor liner (also impingement and effusion cooling without pedestals) when subjected to particulate deposition. It was shown that higher pressure ratios reduced deposition on the surfaces of the holes due to "dirt being pushed through", and higher impingement jet Reynolds numbers also led to reduced deposition heights. In the worst cases, cooling reductions up to 55% from the clean case were observed.

To the authors' knowledge, there is little literature on the effect of the choice of metal alloy on the deposition rate. Notably, a study conducted by Weiwei et al. [18] on the effect of blade roughness on particle deposition in a flue gas turbine showed that the particle deposition rate increased with increased blade roughness.

3. METHODOLOGY

3.1 Experimental Methodology

Experiments were conducted using the Oxford Thermofluids Institute's High Temperature Rig (first described in [19]). Figure 2 shows a line diagram of the facility. A CAD diagram of a Double-Wall test piece in its containment test section is shown in Figure 3. This test section was placed inside the oven (a Wild Barfield M1354 Industrial Furnace), connected to the combined gas path, and sealed in using additional bricks.

The facility operates with pre-dried air supplied at 7 bar. This air is initially filtered through a KFS400-15 filter and then directed into a manifold, which splits the flow into three separate streams, each regulated by OMEGA Mass Flow Controllers. The particulate flow is directed into a solid particle aerosol generator, through which it can entrain particulates at the required concentration. The second is the high temperature flow, which passes through an air heater. The air heater used was a TUTCO SureHeat JET 8kW Air Heater (F074719 [20]) with TUTCO SureHeat Jet Control (F075526 [21]), capable of heating airflows up to 1000 K. These two flows would combine in the mixing chamber and enter the test piece. After exiting the oven, the combined flow from the test piece would be mixed with the dilution flow to reduce its temperature, and then passed through a HEPA filter to avoid the expulsion of harmful particulate matter. All flow rates were controlled by OMEGA mass flow controllers – the heater by an FMA-2612A rated up to 8.33×10^{-3} m^3/s [22], dilution flows by an FMA5545As, rated up to 16.67×10^{-3} m^3/s [23], and the particulate flow by an FMA-2609A, rated up to 0.83×10^{-3} m^3/s [22].

The test pieces themselves were flat plate coupons made up in two parts – one which contained the impingement holes and another which contained the effusion holes. This design allowed the test pieces to be disassembled, giving optical access to the deposition on the inner surfaces. CAD diagrams of a test piece are shown in Figure 4 and Figure 5. The exits of the effusion holes were counterbored to remove any downstream flow influence on deposition. As seen in Figure 3, the combined test piece was placed in a holder to prevent the parts from separating.

The aerosol generator used was a PALAS RBG 1000 IGD [24]. Particle matter was loaded into a cylindrical piston, which was controlled to move upward at a set rate. This would push particles onto a rotating brush, which the air flow passed and would carry particulates on to the mixing chamber. Prior to each set-up of the aerosol generator, the piston was weighed before and after particulates were loaded into it. Knowing the volume occupied by the particulate matter, the difference in masses was used to calculate its density.

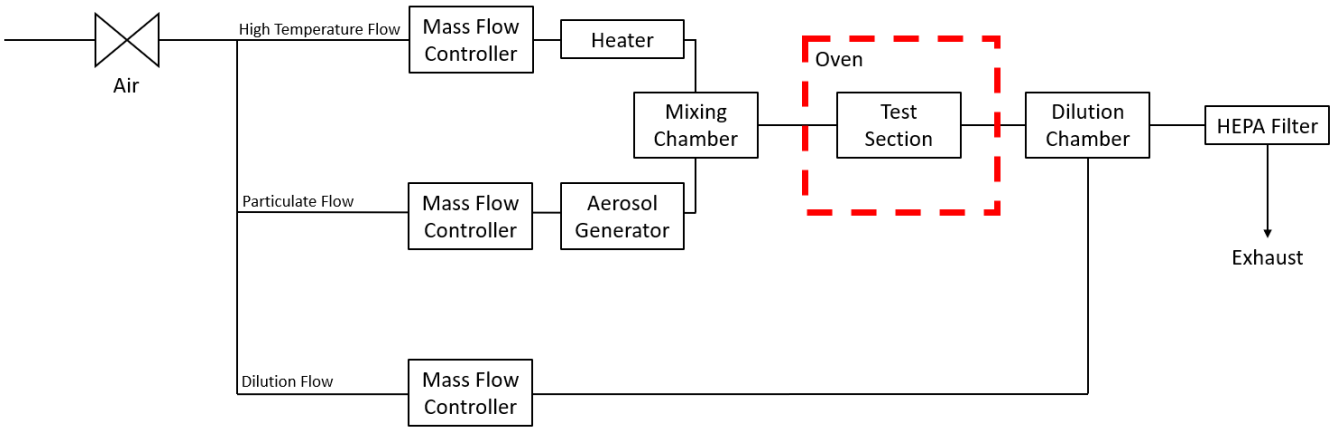

FIGURE 2: DIAGRAM OF THE EXPERIMENTAL FACILITY (ADAPTED FROM [19])

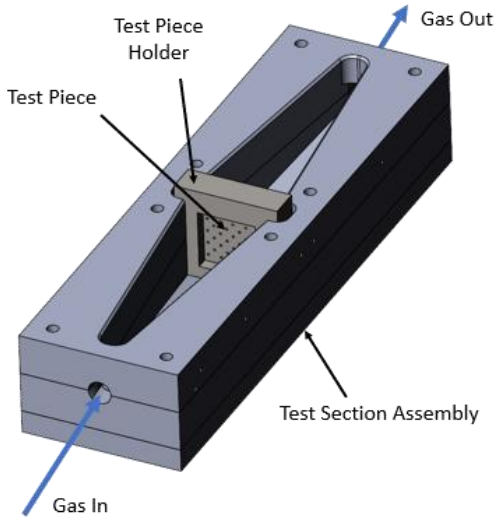

FIGURE 3: CAD MODEL OF THE TEST SECTION ASSEMBLY WITH TOP LID REMOVED

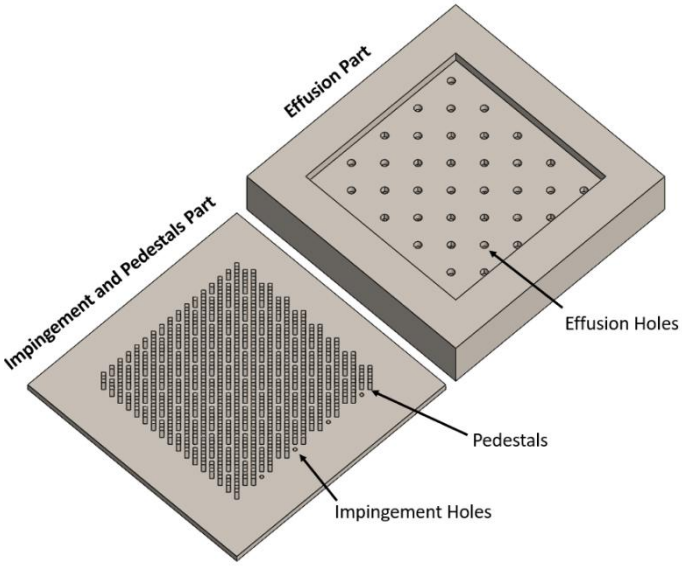

FIGURE 4: CAD MODEL OF THE TWO PARTS OF A TEST PIECE, WITH INTERNAL WALLS FACING UPWARD

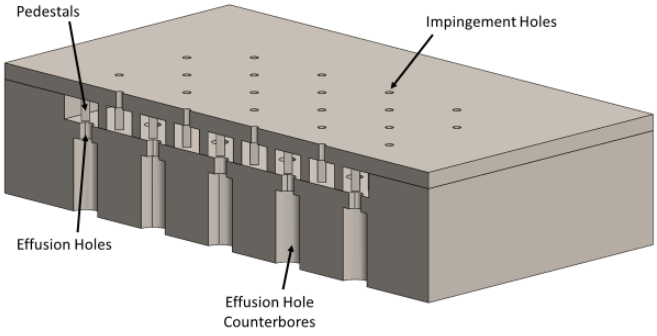

FIGURE 5: CAD SECTION VIEW OF ASSEMBLED TEST PIECE

The steps taken in the general procedure of the experiment were often governed by the average metal temperature of the test section. This was monitored using 6 thermocouples (5 along the side of the test section assemble, 1 on top). A continuous recording of the upstream supply pressure was also used to monitor the experiment. The general procedure for running experiments is laid out below:

1. The mass of the clean test piece was measured. It was then inserted into the test section, and the gas path was assembled.
2. With the gas path assembled and the oven sealed, the oven would be turned on with a set target temperature and all flows were activated. The air heater would run at its maximum temperature to maximise the rate at which the test piece would heat up.
3. Once the average metal temperature of the test section assembly had risen to the target, the heater flow temperature and flow rate were dropped to testing conditions, and ran until a steady state was reached at the target temperature. The testing flow rate was 1.33×10^{-3} m^3/s.
4. The aerosol generator was activated to start pushing particles into its airflow. This was continued until the piston had climbed by a desired amount, i.e. a certain volume of particles had been ejected to flow into the test section. A total volume of approximately 500 mm3 (12.9 mm change in piston height) was targeted to be injected in each test. During the test, the particulate flow rate was 0.42×10^{-3} m^3/s. Combined with the heater flow, this produced a flow Re of approximately 2000 based on the effusion hole diameter.
5. Once particle ejection was complete, the aerosol generator was deactivated, all heat sources turned off and the airflows allowed to run unheated until the rig had cooled down to ~500 K, such that it could be left to cool safely overnight. It would then be disassembled and the test piece removed for inspection.
6. The mass of the test piece would be measured immediately following disassembly. It was then taken to be measured under a microscope.
7. After all measurements were complete, the test piece would be cleaned with compressed air and deionised water for the next test.

Figure 6 shows a test piece following a deposition test. The near side piece is the effusion wall piece – significant mounds of particle deposition are visible at the locations of impingement points. Less concentrated deposition is evident on the impingement and pedestals piece.

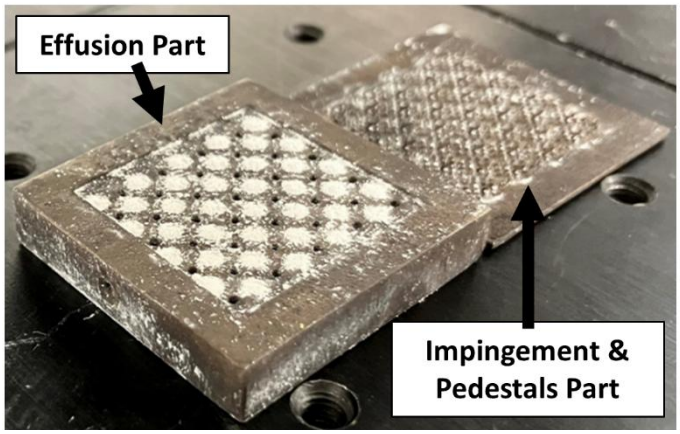

FIGURE 6: D3 STEEL TEST PIECE READY FOR INSPECTION FOLLOWING HOT ARIZONA ROAD DUST DEPOSTION EXPERIMENT

3.2 Test Variables

Four variables were selected to test their influence on particle deposition. The first was temperature – tests were conducted in 'hot' and 'cold' conditions, nominally chosen to have the metal temperature be representative of High-Pressure and Low-Pressure turbine cooling system conditions respectively. In hot conditions, the mean metal temperature was 1150 K. In cold conditions, it was 900 K. In all tests, the gas temperature was set to produce a gas-to-metal temperature ratio of 0.85.

The second variable of interest was the cooling system geometry. These geometries, D3 and D6, were chosen to match those used in the prior computational study by the authors [25]. Both are flat plate Double-Wall Effusion Cooling geometries with diamond shaped pedestals which were first investigated by Murray et al. [26]. The layout of these geometries is shown in Figure 7 in unit cell form, where cells are mirrored and repeated to form the full geometries as shown in Figure 4. The various geometric values for D3 and D6 are listed in Table 1. The only difference between the two geometries is their pedestal lengths (L_p) and impingement hole diameters (D_i), which produced a major difference in the impingement spacing-to-hole-diameter ratio, which was ½ for D3 and 3 for D6. Due to the different hole diameters, the D3 geometry's impingement plate is 4 times as porous as D6's. The full parts each had 36 holes, with 514 pedestals on each Impingement and Pedestals part.

	L_i	L_f	L_p	L_1	L_2	D_i	D_f	s
D3	1.0	1.0	0.5	0.5	0.5	1.0	1.0	2.82
D6	1.0	1.0	1.5	0.5	0.5	0.5	1.0	2.82

TABLE 1: UNIT CELL DIMENSIONS. ALL IN MM.

The third variable used was the composition of the particulate matters themselves. Two types were used: Arizona Road Dust (ARD) and Manchester University's Test Dust 50 (TD50). Specifications of ARD go back to the 1940s and are representative of dust samples taken in Arizona's Salt River Valley [27]. For these tests, an A1 ultrafine version of ARD was used [28]. As TD50 was developed to represent dusts ingested in the Middle East [13], the comparison of these two particulate matters' deposition rates gives a useful contrast of deposition rates between two continents. Table 2 summarizes the properties of the two particulate matters used – for ARD, the standard ISO 12103-1 is used. Information for TD50 is based on estimates from the work of Elms et al. [13].

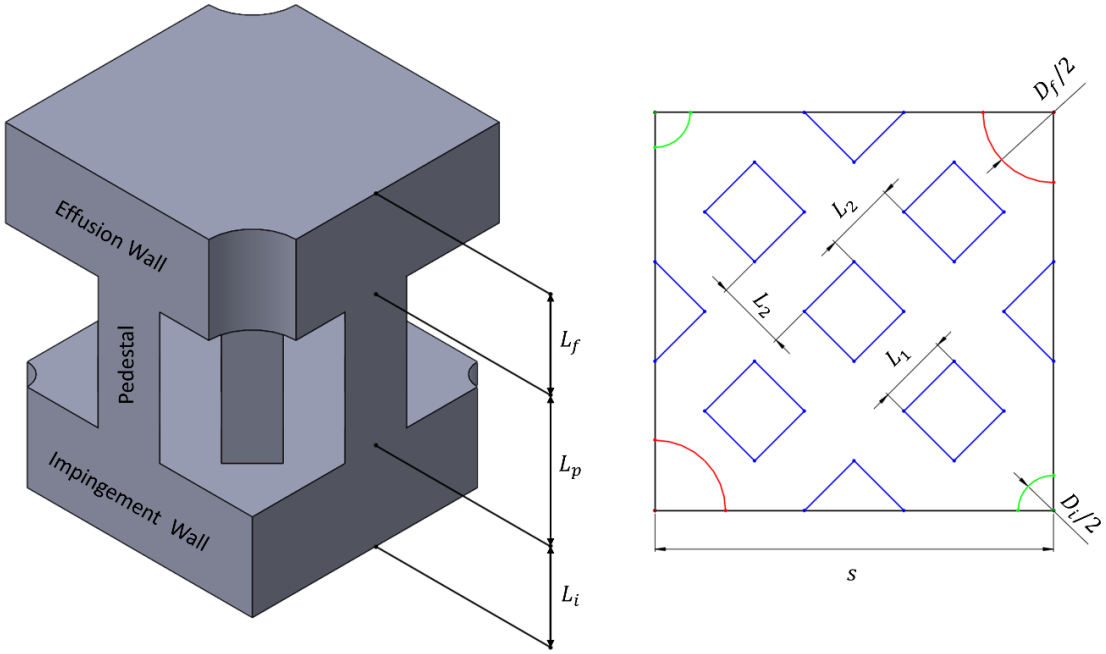

FIGURE 7: (A) CAD DIAGRAM OF UNIT CELL SHOWING WALL THICKNESSES AND PEDESTAL LENGTH & (B) UNIT CELL LAYOUT SHOWING SIZING OF INTERNAL FEATURES

Particulate Matter	ARD	TD50
Median Particle Size	5.5 µm	14 µm
Largest Particle Size	22 µm	47 µm
Mean Packing Density in Piston	730 kg/m^3	1150 kg/m^3
In-Test Concentration	150 mg/m^3 air	230 mg/m^3 air
Composition (minerals of significant proportion)	69 - 77% Quartz 8 - 14% Al_2O_3 4 - 7% Fe_2O_3 2.5 - 5.5% CaO 2 – 5% K_2O	~30% Dolomite ~25% Calcite ~20% Na-montmorillonite ~5% Gypsum ~5% Halite ~5% Quartz

TABLE 2: PARTICULATE MATTER PROPERTIES

It must be noted that the In-Test Particle Concentrations are far higher than would be expected in standard operating conditions. This was done to ensure sufficient particle deposition for measurement that could be accomplished within a reasonable timeframe. Similar practices were employed by Jensen et al. [29], who conducted deposition tests for a single jet impinging on a coupon. By increasing the in-air particle concentration, the authors were able to simulate 10,000 hours of standard land-based turbine deposition in a 4 hour test, and found that the surface topography was very similar to the engine-ran blades. As such, it is taken in this study that it is the overall amount of particulate matter delivered that is key to deposition, rather than its concentration.

The final variable investigated was the specific metal alloy. Whilst the original D3 and D6 test pieces were manufactured from stainless steel, an additional D3 test piece was manufactured from the nickel superalloy CMSX-4.

3.3 Measurement Methodology

Deposition was measured using two methods for these experiments. Mass deposition was measured as the change in mass of the test piece over the course of the experiment – as such, the test piece's two parts would be weighed before and after each test using a Sartorius ENTIS 6231-1S scale [30], with precision to the thousandth of a gram. The same scale was used to find the mass of particulate matter in the piston as described in Section 3.1.

The second assessment of deposition was based on the volume of deposited particle matter. This was investigated using an Alicona G4 InfiniteFocus Profilometer [31]. This microscope was used to evaluate the variation in surface height across the inner walls of test pieces. With a reference clean spot datapoint taken, this process effectively allows the height of deposition mounds at each point to be assessed. Profile scans were performed at increments of 2.6094 µm. This 3D dataset would then be imported into MATLAB to carry out a numerical integration for the volume of particulate matter deposited, using the midpoint rule [32]. This can be used to estimate the definite integral of a function $f(x)$ over an interval $[a, b]$. If the interval is divided into n subintervals of length $\Delta x = (b-a)/n$, the midpoint of the i^{th}subinterval is m_i and the midpoint rule can be defined as:

$$M_n = \sum_{i=1}^{n} f(m_i)\Delta x \quad such\ that \lim_{n\to\infty} M_n = \int_a^b f(x)\ dx \tag{2}$$

When considering a volume, the equation is simply modified to reflect the volume below a z coordinate:

$$V \approx \sum_{i=1}^{n}\sum_{j=1}^{m} z(x_i, y_j)\,\Delta x\,\Delta y \tag{3}$$

As $\Delta x = \Delta y = 2.6094\ \mu m$, the error of the midpoint rule in the approximation to the area was assumed to be small.

Throughout experiments, the pressures of selected flow positions were recorded, as well as temperatures of the flows and the test section using high pressure thermocouples. Readings were made for all positions at a rate of 10 Hz, but due to the long runtime of the experiment these were averaged over 10 s intervals to be logged.

3.4 Measurement Uncertainty

The uncertainties of the measurement instrument used for the assessment of mass and volume deposition are summarised in Table 3 below:

Quantity	Uncertainty
Pressure	± 0.25% of Transducer Range
Temperature	± 5 K
Mass (Test Piece, Dust)	± 0.6 mg
Initial Particulate Depth (Used for Powder Density)	± 1 mm
Piston Position	± 0.1 mm
Particulate Air Flow Rate	± 2.5 × 10^{-6} m^3/s
Heater Air Flow Rate	± 5 × 10^{-6} m^3/s
Deposit/Roughness Height	± 0.5 µm

TABLE 3: UNCERTAINTIES OF MEASUREMENTS

Uncertainties for the mass and volume deposition, evaluated as the proportions of particulate mass and volume deposited in the test respectively, are calculated per Moffat [33], where the uncertainty for any property i derived from n measured properties j with is given by Eq. (4).

$$U_i = \sqrt{\left(\sum_{j}^{n}\left(\frac{\partial i}{\partial j}\right)^2 {U_j}^2\right)} \tag{4}$$

4. RESULTS AND DISCUSSION

4.1 Surface Roughness Results

Prior to testing, each test piece was examined under the microscope to find the arithmetic mean roughness, R_a, as defined in Eq. (5), where n is the number of measurements taken. These results are shown in Table 4. It must be noted that the steel test pieces were additively manufactured and had been used in experimental campaigns before this study, whereas the CMSX-4 test piece was newly cast and machined. This likely contributed to the steel test pieces having the rougher surfaces.

$$R_a = \frac{1}{n}\sum_{i=1}^{n}|z_i - \bar{z}| \quad (5)$$

Test Piece	R_a
D3, Steel	0.01426 ± 0.0005
D6, Steel	0.00488 ± 0.0005
D3, CMSX-4	0.00246 ± 0.0005

TABLE 4: ARITHMETIC MEAN ROUGHNESSES OF TEST PIECES, ALL IN MM

4.2 Mass Deposition Results

Mass Deposition is evaluated in terms of the rise in test piece mass as a proportion of the total mass of particulate matter ejected into the gas path. These results for all tests are shown in Figure 8, separated to demonstrate the effects of temperature, cooling geometry, particulate matter, and metal alloy independently. Each datapoint shows the result of a single test. Select tests were repeated with relatively consistent results.

Firstly, reviewing the results of the effect of temperature, it is clear that hotter conditions produced greater particulate deposition, with the exception of the D3/TD50/CMSX-4 pair of tests. This is the trend that would be expected and aligns with results in the literature – hotter conditions soften the particulate matter, significantly increasing the potential of particle adhesion to the surface as they become glassier and stickier [34]. On average, in hot conditions there was 2.09% more deposition compared to their cold counterparts (i.e. a 2.09% increase in capture efficiency). The discrepant test point could have several potential causes, such as the test piece moving out of position during the test or percussive impacts during the disassembly of the experimental facility.

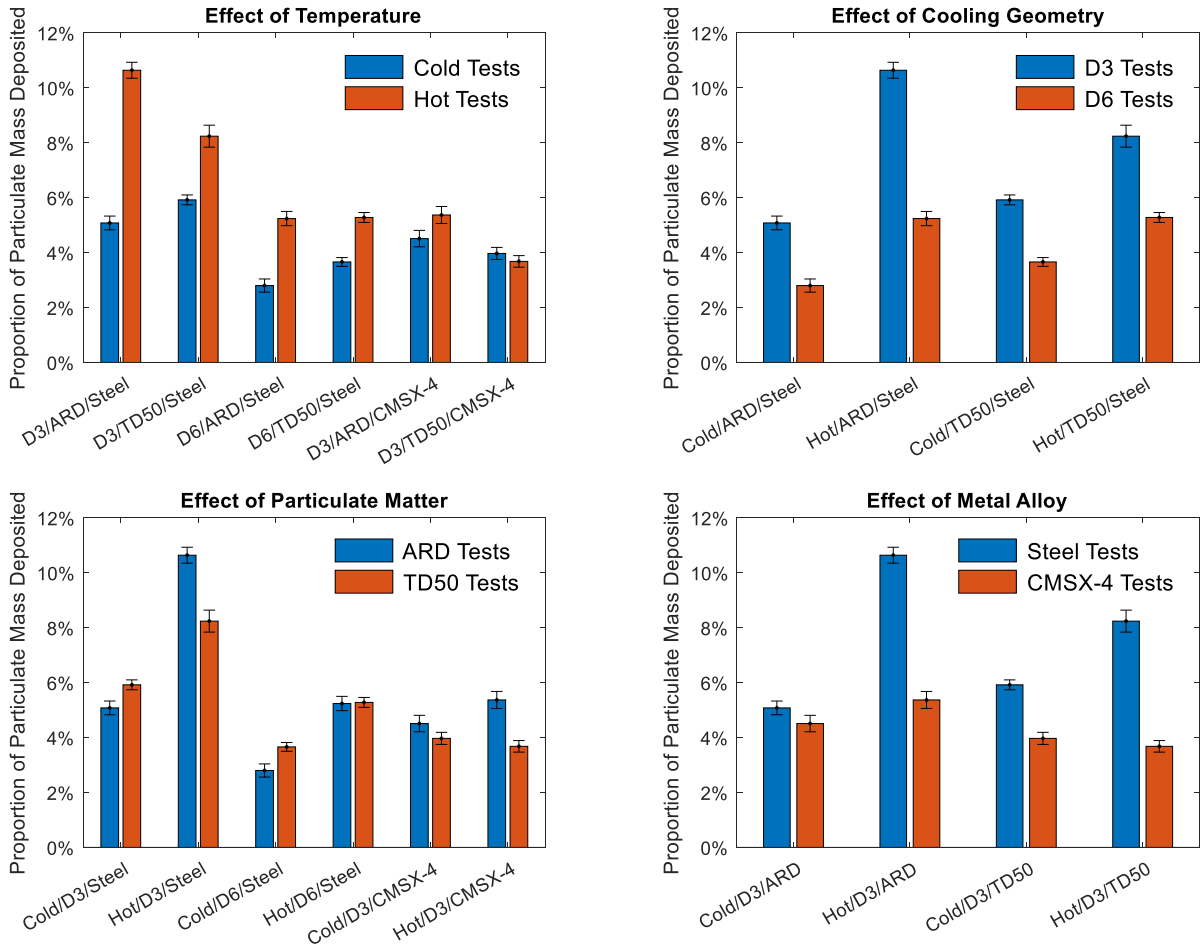

FIGURE 8: PROPORTION OF PARTICLULATE MASS DEPOSITED IN ALL TESTS, COMPARING THE EFFECTS OF (A) TEMPERATURE, (B) COOLING GEOMETRY, (C) PARTICULATE MATTER, AND (D) METAL ALLOY

The effect of cooling geometry is clearly evident, with the D3 geometry leading to greater deposition than the D6 across all tests, with an average of 3.23% more mass deposition. Two key elements must be considered here – the differences in impingement wall porosity, and in the impingement spacing to diameter ratio. Due to the equal flow rate and similar inlet pressures of the two test pieces, impingement jets in the D6 geometry would be expected to have a significantly greater velocity than those in D3, making them more effective at breaking up particle deposits as per [16].

As the test piece was made up of separate parts for the impingement wall and effusion wall, the amount of deposition could be weighed separately, for which notable differences were clear between the results of the two geometries. These are shown in Figure 9, where it is plain that a far greater share of the total deposition occurred on the impingement and pedestals part for D6 compared to D3. For D3, the vast majority of deposition always took place on the effusion part. These results align with previous reasoning – more particulates are likely to be swept away from the target wall by the faster impingement jet of D6, essentially leaving more particles to potentially deposit on the pedestal surfaces. The smaller impingement hole of D6 may also be a cause of greater deposition on the upstream facing surface of the impingement plate. Of course, the overall deposition remains much greater for D3, which highlights the prevalence of impingement-based particle deposition in these systems.

The effect of the particulate matter chosen appears to have no consistent effect (though ARD mass deposition was on average 0.48% greater than TD50). There is likely contrasting forces at play here, where the physics dependent on particle size must be considered alongside the chemistry of the different particulate matters and differences in softening temperatures of different components. Unfortunately, this is outside the scope of this paper.

Finally, the metal alloy comparison shows greater deposition for all steel tests compared to CMSX-4 tests (3.09% more on average). It is hypothesised that this may have been due to surface roughness effects, rather than the metal alloy itself. Results from Section 4.1 show that for the D3 components, the steel component was nearly 6 times rougher than the CMSX-4 part. As literature sources generally suggest that higher surface roughness enhanced deposition (see [18]), it logically follows that the rougher steel test piece experienced greater deposition than its smoother CMSX-4 counterpart.

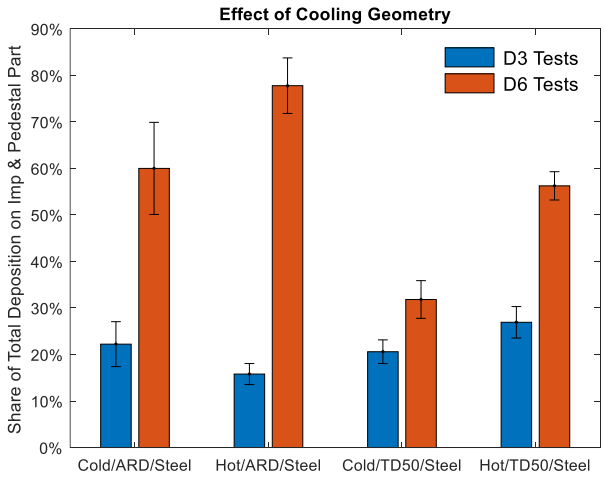

FIGURE 9: SHARE OF TOTAL DEPOSITION ON THE IMPINGEMENT & PEDESTALS PARTS, COMPARED FOR DIFFERENT GEOMETRIES

Comparing the results of these experiments to those of Villain et al. [25], where the deposition of ARD on the D3 and D6 geometries was assessed computationally, relatively similar trends are observed. For 5 µm particles passing through the D3 geometry at low Re comparable to these tests, the authors predicted that the vast majority of deposition would take place on the target surface (the internal surface of effusion wall), with an increasingly large proportion sticking to the impingement wall's inner surface as the flow Re increased, aligning with the findings of [16]. For the same sized particles passing through D6, Villain et al. [25] predicted that the majority of deposition would take place on the pedestals and the internal facing surface of the impingement plate, with a smaller proportion taking place on the target surface on the effusion wall. These results were almost insensitive to Re and align well with the ARD tests shown in Figure 9.

4.3 Volume Deposition Results

As the density of the particulate matter is likely to change during the high temperature deposition process, the volume of deposited particulate matter is considered independently of the mass of deposited matter. It is the volume of deposits which is arguably more significant in terms of blockage of the cooling system, particularly when clumped deposits are present.

Unfortunately, as the deposition patterns on the Impingement and Pedestal part tended to be highly spread out, discerning between deposition and the surface roughness of the part proved to be too slow a process for effective data collection, and as such results are only shown for the Effusion Parts. As shown in Figure 6, it was at the impingement points on the target plate where the largest clumps of deposited material appeared. Due to the same time constraints, scans of the deposited material on the target surface were made of a central section of the effusion test piece, covering approximately 5 impingement-location clumps of deposited material. The volume measured in these sections was extrapolated across the area of the target surface to estimate the total volume of deposited particulate matter on the target plate. An example of a scanned target surface is shown for the Hot/D3/ARD/Steel test in Figure 10.

Figure 11 shows how the proportion of total particulate volume deposited on the target surface varies with temperature, cooling geometry, particulate matter, and metal alloy. As would be expected, general trends follow those of the mass deposition, where volume deposition is 0.74% greater for hot tests than cold ones, 1.48% greater for the steel parts compared to the CMSX-4 ones, and 0.61% greater for ARD tests compared to TD50 ones.

As this assessment is for the effusion part only (and a greater share of deposition was previously found to take place on the

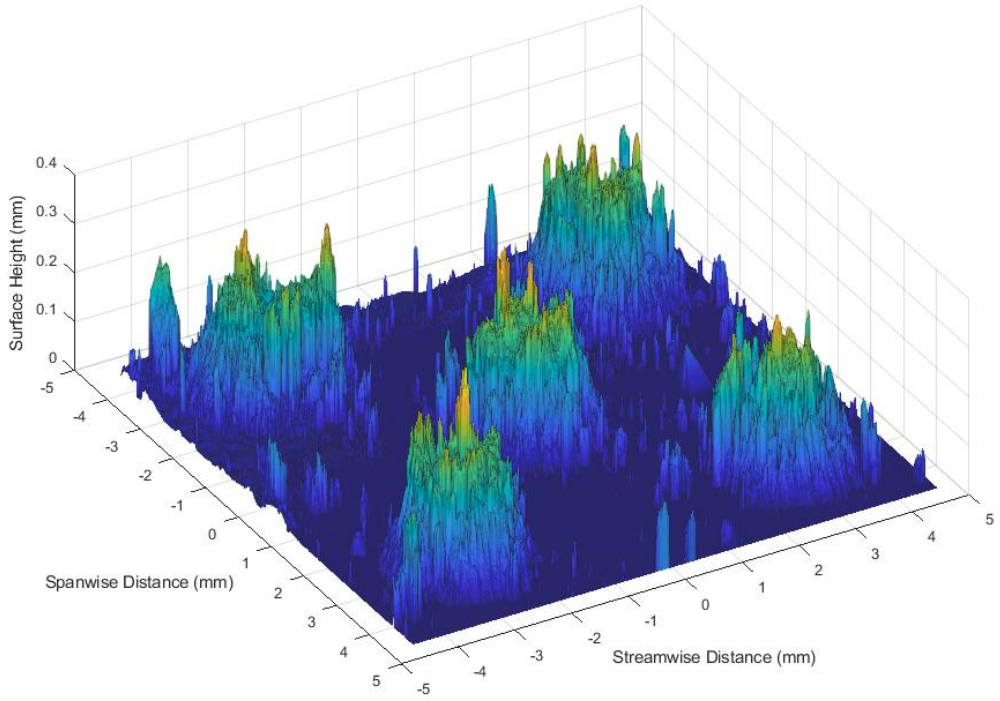

FIGURE 10: DEPOSITION ON THE TARGET SURFACE OF THE EFFUSION PART FOR HOT/D3/ARD/STEEL

impingement and pedestals part for D6), significantly greater deposit volumes were observed for the D3 geometry – 2.35% higher volume deposition on average. Indeed, for the vast majority of tests, the build-up of deposited particulate matter was in a similar pattern to that seen in Figure 6, where deposition on the target surface forms shapes resembling molehills at the impingement points. Whilst not perfectly symmetrical, it was found that these molehill-shaped deposition mounds were the location of greatest deposition height. The maximum and mean deposition heights across the target surface are compared for the two different cooling geometries in Figure 12. It should be noted that the volume injected was manually controlled, and thus had slight variations due to user timing. Deposition heights have been corrected to the intended reference volume to compensate for this. As has been discussed, the faster impingement jet of the D6 geometry breaks up the build-up of deposits in this location, leading to much lower heights of deposition mounds. Notably, the two geometries come closest in the Cold/TD50/Steel set of tests - it was only in this configuration where the majority of deposition occurred on the effusion part for a D6 test, as shown in Figure 9.

For the D3 results, particularly the Hot/ARD/Steel one, the findings may pose application challenges – the deposition height of 0.38 mm is 77% of the distance between the impingement hole's exit and the target surface. The amount of ARD injected in this test is approximately 0.35 g. If an aeroengine is assumed to use 100 kg/s of air during a take-off run which lasts an average of 30 s, approximately 0.09 g of ARD will be ingested (using a particle concentration of 30 µg/m^3 of air). If 5% of the core flow is used for cooling of 80 blades and distributed evenly, a panel like the test pieces used may use 20% of this – this gives a total ARD mass of 11 µg per take off. As such, the test mass represents approximately 32,000 take-off cycles. Of course, this analysis has used a large number of assumptions, and there would be particle ingestion throughout the flight cycle (albeit of different concentrations), but the number of cycles to blockage appears too high to be of major concern. However, if the average particle concentrations ingested were to rise to those seen in regions with high pollution or prone to dust storms, blockage-related concerns could arise quickly. Reduction in cooling performance, as demonstrated by McFerran et al. [17], would also need to be seriously considered when atmospheric particle concentrations are consistently high.

To look further into the deposition patterns at the impingement point, the circumferentially averaged height of the deposition mounds were compared for the ARD tests of the two geometries, shown in Figure 13. These averages were taken for the mounds featuring the highest deposition height, although these positions generally did not lie on the impingement point itself. The influence of the geometry is clear, and follows on from the results shown in Figure 12. Notably, hot conditions in the D6 geometry do not seem to drastically increase the maximum height of the deposition mound, but rather cause it to bulk out. For the D6 geometries, the deposited particles appear to be more spread out from the impingement point, depositing with the expansion of the radial wall jet.

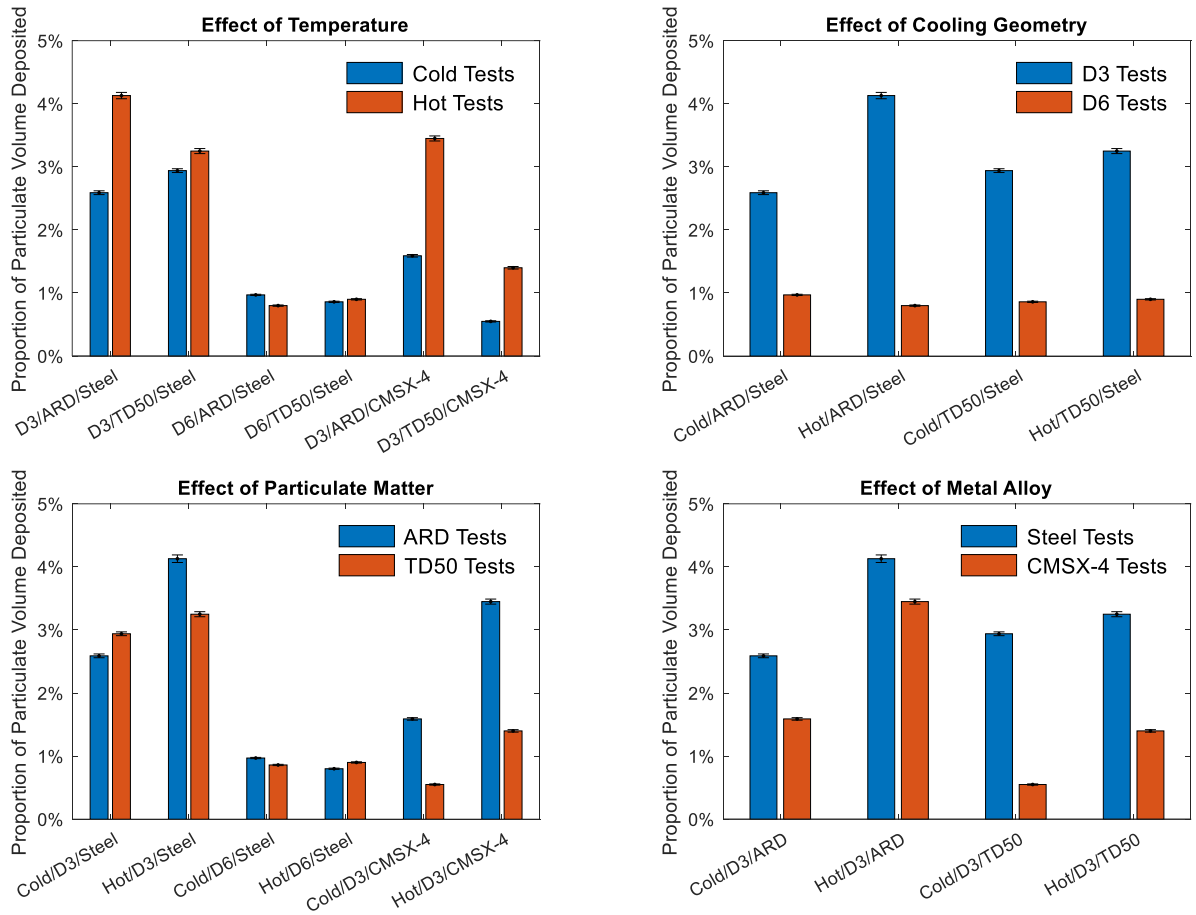

FIGURE 11: PROPORTION OF PARTICLULATE VOLUME DEPOSITED ON THE TARGET SURFACE IN ALL TESTS, COMPARING THE EFFECTS OF (A) TEMPERATURE, (B) COOLING GEOMETRY, (C) PARTICULATE MATTER, AND (D) METAL ALLOY

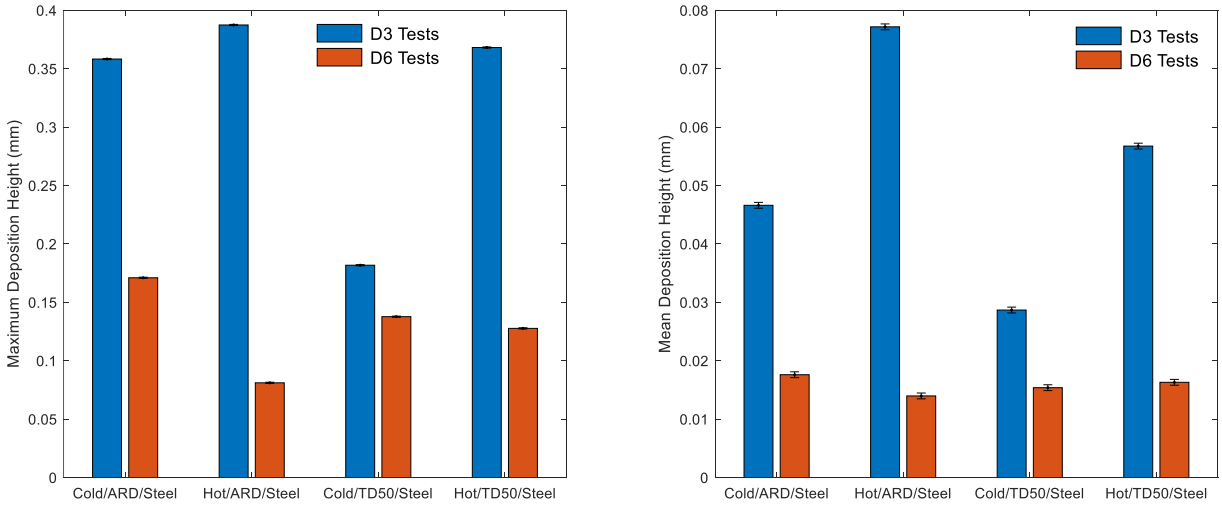

FIGURE 12: MAXIMUM AND MEAN DEPOSITION HEIGHTS, COMPARED FOR DIFFERENT GEOMETRIES

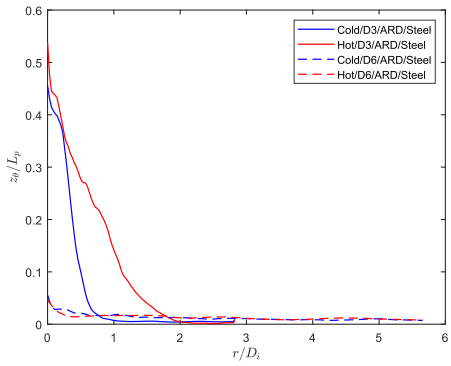

FIGURE 13: NORMALISED CIRCUMFERENTIALLY AVERAGED DEPOSTION HEIGHTS FOR IMPINGEMENT MOUNDS

5. CONCLUSION

The vulnerability of Double-Wall Effusion Cooling Systems to particle deposition has been assessed through experimental methods at high temperatures. The influence of temperature, cooling geometry, particle matter composition, and metal alloy on the mass and volume of deposited particulate matter has been investigated. The amount of particle deposition was seen to generally increase in hotter conditions, and for the geometry with a small impingement spacing to diameter ratio and high impingement wall porosity. The stainless steel test piece produced higher levels of particle deposition than the CMSX-4 test piece, but this could be a product of its higher surface roughness. Finally, no consistent trend was observed for the influence of the particle matter composition of what proportion of its mass was deposited.

In select test cases, the amount of particle deposition was significant enough to suggest that Double-Wall Effusion Cooling Systems could be susceptible to complete blockage by particle deposition within their expected life, if they consistently experience a very high level of atmospheric particle concentration. In these cases, the growth of molehill-shaped deposition patterns at the impingement point could cause mountain-sized problems. More standard levels of particle concentration, however, will pose much less of a threat.

Future research will look into extending the case studies examined. In particular, the temperature range will be expanded to match the hotter engine conditions, and the facility upgraded to handle higher air flow rates and absolute pressures. Sacco et al. [35] showed that higher values of absolute pressure for a fixed pressure ratio reduced particle capture efficiency for an impinging jet, and this experiment's value would increase if it could be engine-representative.

6. ACKNOWLEDGEMENTS

Thanks go to the Oxford Materials Characterisation Service for measurements of TD50. This work is supported by Rolls Royce plc., UKRI and the EPSRC under the CDT in Future Propulsion and Power (UKRI Ref. EP/S023003/1) and CORDITE (UKRI Ref. 75107).

7. REFERENCES

[1] J.-C. Han, "Fundamental Gas Turbine Heat Transfer," *Journal of Thermal Science and Engineering Applications,* vol. 5, no. 2, 2013.

[2] R. S. Bunker, "Evolution of Turbine Cooling," in *ASME Turbo Expo 2017: Turbomachinery Technical Conference and Exposition*, Charlotte, North Carolina, 2017.

[3] A. V. Murray, P. T. Ireland and A. J. Rawlinson, "An Integrated Conjugate Computational Approach for Evaluating the Aerothermal and Thermomechanical Performance of Double-Wall Effusion Cooled Systems," in *ASME Turbo Expo 2017: Turbomachinery Technical Conference and Exposition*, Charlotte, North Carolina, 2017.

[4] M. van de Noort, A. V. Murray and P. T. Ireland, "Low Order Heat & Mass Flow Network Modelling for Quasi-Transpiration Cooling Systems," in *ASME Turbo Expo 2022*, Rotterdam, The Netherlands, 2022.

[5] M. Courtis and P. T. Ireland, "Influence of Porosity on Double-Walled Effusion-Cooled Systems for Gas Turbine Blades," in *ASME Turbo Expo 2022: Turbomachinery Technical Conference and Exposition*, Rotterdam, The Netherlands, 2022.

[6] J. Zhang, H. Huaizhi, Z. Li and H. Zhong, "Influence of pin-fin height and diameter on flow and cooling characteristics of three-layer porous laminates: an experimental study," *Experimental Heat Transfer,* vol. 35, no. 6, pp. 884-899, 2022.

[7] K. K. Ferster, K. L. Kirsch and K. A. Thole, "Effects of Geometry, Spacing, and Number of Pin Fins in Additively Manufactured Microchannel Pin Fin Arrays," *J. Turbomach.,* vol. 140, no. 1, 2018.

[8] H. S. Song, H. S. Park, T. Kim, S. Choi, H. Moon and H. H. Cho, "Cooling Effectiveness of Additive-Manufactured Internal Structure Within a Double Wall Cooling System," in *ASME Turbo Expo 2023: Turbomachinery Technical Conference and Exposition*, Boston, Massachusetts, 2023.

[9] A. Suman, N. Casari, E. Fabbri, M. Pinelli, L. di Mare and F. Montomoli, "Gas Turbine Fouling Tests: Review, Critical Analysis, and Particle Impact Behavior Map," *J. Eng. Gas Turbines Power,* vol. 141, no. 3, 2018.

[10] J. M. Crosby, S. Lewis, J. P. Bons, W. Ai and T. H. Fletcher, "Effects of Temperature and Particle Size on Deposition in Land Based Turbines," *J. Eng. Gas Turbines Power,* vol. 130, no. 5, 2008.

[11] C. Bonilla, J. Webb, C. Clum, B. Casaday, E. Brewer and J. P. Bons, "The Effect of Particle Size and Film Cooling on Nozzle Guide Vane Deposition," *J. Eng. Gas Turbines Power,* vol. 134, no. 10, 2012.

[12] T. M. Wolff, C. P. Bowen and J. P. Bons, "The Effect of Particle Size on Deposition in an Effusion," in *2018 AIAA Aerospace Sciences Meeting*, Kissimmee, Florida , 2018.

[13] J. Elms, A. Pawley, N. Bojdo, M. Jones and R. Clarkson, "Formation of High-Temperature Minerals From an Evaporite-Rich Dust in Gas Turbine Engine Ingestion Tests," *J. Turbomach.,* vol. 143, no. 6, 2021.

[14] E. D. Crowe and J. P. Bons, "Effects of Dust Composition on Particle Deposition in an Effusion Cooling Geometry," in *ASME Turbo Expo 2019: Turbomachinery Technical Conference and Exposition*, Phoenix, Arizona, 2019.

[15] J. P. Bons, C. Lo, E. Nied and J. Han, "The Effect of Gas and Surface Temperature on Cold-Side and Hot-Side Turbine Deposition," *J. Turbomach.,* vol. 144, no. 12, 2022.

[16] C. C. Land, C. Joe and K. A. Thole, "Considerations of a Double-Wall Cooling Design to Reduce Sand Blockage," *J. Turbomach.,* vol. 132, no. 3, 2010.

[17] K. McFerran, K. A. Thole and S. P. Lynch, "Dirt Ingestion Impacts on Cooling Within a Double-Walled Combustor Liner," in *ASME Turbo Expo 2024: Turbomachinery Technical Conference and Exposition*, London, United Kingdom, 2024.

[18] X. Weiwei, Z. Konghao, W. Jianjun, L. Yajun and L. Qiang, " Modeling and numerical analysis of the effect of blade roughness on particle deposition in a flue gas turbine," *Powder Technology,* vol. 347, pp. 59-65, 2019.

[19] N. Vadgama, S. Beal, P. Forsyth, M. McGilvray and D. Gillespie, "Experimental Deposition of Particulates in Accelerating Flows at Engine Representative Conditions," in *AIAA AVIATION 2020 FORUM*, Virtual, Online, 2020.

[20] TUTCO SureHeat, "Jet Air Heaters," TUTCO SureHeat, 7 10 2024. [Online]. Available: https://www.tutcosureheat.com/product/jet-air-heaters. [Accessed 7 10 2024].

[21] TUTCO SureHeat, "JET Control Panel Model F075526," 7 10 2024. [Online]. Available: https://www.tutcosureheat.com/images/uploads/technical_bulletins/Datasheet_-_F075526_-_Jet_Control.pdf. [Accessed 7 10 2024].

[22] OMEGA, "Mass and Volumetric Gas Flow Controllers For Clean Gases: FMA-2600A Series," 7 10 2024. [Online]. Available: https://br.omega.com/omegaFiles/green/pdf/FMA2600_FVL2600.pdf. [Accessed 7 10 2024].

[23] OMEGA, "ECONOMICAL GAS MASS FLOW CONTROLLERS For Clean Gases With Optional Integral Display: FMA5400A and FMA5500A," OMEGA Engineering Inc., 7 10 2024. [Online]. Available: https://br.omega.com/omegaFiles/green/pdf/FMA5400A_5500A.pdf. [Accessed 7 10 2024].

[24] Palas GmbH, "RBG 1000 IGD," 4 10 2024. [Online]. Available: https://www.palas.de/en/product/rbg1000igd. [Accessed 4 10 2024].

[25] F. Y. A. Villain, N. Vadgama, J. G. Gaskell, P. T. Ireland, M. McGilvray and D. R. H. Gillespie, "Numerical Investigation of Particle Deposition in Double Wall Effusion Cooled Systems," in *ASME Turbo Expo 2022: Turbomachinery Technical Conference and Exposition*, Rotterdam, Netherlands, 2022.

[26] A. V. Murray, P. T. Ireland and E. Romero, "Experimental and Computational Methods for the Evaluation of Double-Wall, Effusion Cooling Systems," *ASME. J. Turbomach.,* vol. 142, no. 11, 2020.

[27] Powder Technology Inc., "EARLY ARIZONA TEST DUST HISTORY," Powder Technology Inc., 7 10 2024. [Online]. Available: https://www.powdertechnologyinc.com/test-dust-history/early-arizona-test-dust-history/. [Accessed 7 10 2024].

[28] DMT-Group, "PTI Arizona Test Dust A1 ultrafine," DMT-Group, 7 10 2024. [Online]. Available: https://testdust.dmt-group.com/en/standard-test-dust/161/pti-arizona-test-dust-a1-ultrafine. [Accessed 7 10 2024].

[29] J. W. Jensen, S. W. Squire, J. P. Bons and T. H. Fletcher, "Simulated Land-Based Turbine Deposits Generated in an Accelerated Deposition Facility," *J. Turbomach,* vol. 127, no. 3, 2005.

[30] Satorious Germany, "Entris Laboratory Balances," 1 2 2017. [Online]. Available: https://www.dataweigh.com/media/14445/sartorius-entris-user-manual.pdf. [Accessed 8 10 2024].

[31] University of Southampton, "Alicona G4 InfiniteFocus," Alicona Imaging GmbH, 22 11 2024. [Online]. Available: https://www.southampton.ac.uk/engineering/research/facilities/360/nCATS_facility/alicona.page#%0A_____technical_specifications%0A_____. [Accessed 22 11 2024].

[32] G. Strang and E. Herman, "Numerical Integration - Midpoint, Trapezoid, Simpson's rule," LibreTexts Mathematics, 2021 7 25. [Online]. Available: https://math.libretexts.org/Courses/Mount_Royal_University/MATH_2200%3A_Calculus_for_Scientists_II/2%3A_Techniques_of_Integration/2.5%3A_Numerical_Integration_-_Midpoint%2C_Trapezoid%2C_Simpson's_rule. [Accessed 7 10 2024].

[33] R. J. Moffat, "Describing the uncertainties in experimental results," *Experimental thermal and fluid science,* vol. 1, no. 1, pp. 3-17, 1998.

[34] M. Slaoui, "Particle Deposition in Gas Turbine Engines: The Effect of Temperature," Undergraduate Thesis, The Ohio State University, 2022.

[35] C. Sacco, C. Bowen, R. Lundgreen, J. P. Bons, E. Ruggiero, J. Allen and J. Bailey, "Dynamic Similarity in Turbine Deposition Testing and the Role of Pressure," *J. Eng. Gas Turbines Power,* vol. 140, no. 10, 2018.